Article

Control Synchronization Design of a Multiple Electrohydraulic Actuator System with Linearization Dynamics and an External Disturbance Observer

Jun Qi [1], Qing Guo [2,*], Hualong Ren [3], Zhenlei Chen [4], Yao Yan [2,*] and Dan Jiang [5]

1   School of Automation, Chengdu University of Information Technology, Chengdu 610225, China
2   School of Aeronautics and Astronautics, University of Electronic Science and Technology of China, Chengdu 611731, China
3   School of Culture and Tourism, Sichuan Vocational and Technical College, Suining 629000, China
4   School of Automation Engineering, University of Electronic Science and Technology of China, Chengdu 611731, China
5   School of Mechanical and Electrical Engineering, University of Electronic Science and Technology of China, Chengdu 611731, China
*   Correspondence: guoqinguestc@uestc.edu.cn (Q.G.); y.yan@uestc.edu.cn (Y.Y.)

Abstract: The control synchronization of multiple electrohydraulic actuators (MEHAs) is initially discussed to ensure the consensus of every electrohydraulic actuator (EHA) with three-order isomorphic dynamics. First, the EHA model is linearized using the Lie derivative method to obtain the state-space model of MEHAs. Then, the disturbance observer is used to estimate and compensate for the unknown external load caused by the driving force of a motion plant. Via the Lyapunov technique, this protocol asymptotically achieves consensus to a zero neighborhood with the ultimate boundaries of the MEHAs' state errors. The effectiveness of the synchronous control protocol is verified by both simulation and experimental benches with two-node EHAs.

Keywords: multiple electrohydraulic actuators; synchronous control protocol; disturbance observer; feedback linearization

1. Introduction

An electrohydraulic servo system (EHSS) represents a popular driving actuator used in some areas of mechanical engineering such as hydraulic exoskeletons [1], hydraulic bouncing systems [2], quadruped robotics [3], hydraulic manipulators [4], shaking tables [5], etc. Previous works on EHSS and other mechatronics focused on uncertain parametric estimations [6–10] and external load compensations [11–16]. By not addressing the uncertainty and external load, the EHSS output performance will decline. In addition, some uncertainties and disturbances are well handled in pneumatic loading systems [17] and electric power systems [18] by using adaptive control and data-mining technologies. Furthermore, some parallel mechanisms driven by multiple electrohydraulic actuators, such as shaking tables [19] and spatial electrohydraulic robots [20], are more challenging for realizing collaborative control since the coupling nonlinearity should be addressed in advance.

The problem of the synchronous control of multiple EHSSs was initiated by Jafari et al. [21]. The author proposed a distributed average consensus protocol used in the velocity control loop of four EHSS nodes. This is the first time that multiagent control theory and network topology has been integrated into an EHSS plant. Actually, distributed multiagent cooperation [22] has recently garnered a lot of attention in the information domain, such as formation spacecraft flight [23], distributed sensor networks [24], and collaborative surveillance [25]. Nowadays, the distributed consensus is a fundamental problem for multiagent collaborative control, which is closely related to formation control [26] and flocking problems [27]. The consensus protocol is designed to guarantee that many agents

achieve an agreement on finite quality. In the past twenty years, many researchers have studied multiagent consensus problems from different perspectives and written several papers. For example, a theoretical framework for the consensus algorithms [28] was designed in multiagent network systems based on modern control techniques, matrix theory, and algebraic graphs. Meanwhile, the cooperative control of autonomous mobile agents [29] was studied with multiple leaders using different interconnection methods. To address the consensus of multiagent systems with general linear and Lipschitz nonlinear dynamics, Li et al. [30,31] presented both distributed adaptive static and dynamic consensus controllers. Subsequently, an adaptive robust NN control for every node was given in [32] to address the tracking consensus for nonlinear systems with high-order dynamics. In addition, the consensus problem of directed multiagent networks [33] was discussed with a variable delay and intrinsic nonlinear dynamics. The finite-time consensus issue of multiagent systems was considered in [34]. The necessary and sufficient conditions for common linear and a two-order multiagent consensus [35,36] were derived to solve the linear multiagent consensus problem. Many distributed consensus algorithms [37–39] were often handled by linear matrix inequality to achieve consensus. Considering switch control theory, Wen et al. [40] provided proof that a multiagent system's consistency with a spanning tree could be converted into the stability proof of many low-dimensional systems. Meanwhile, the consensus algorithm was also proposed in the smallest real part of the Laplacian matrix with non-zero eigenvalues [41–43], which adopted both its own and its neighbors' local data. To avoid known global data of the Laplacian matrix, adaptive consensus protocols were presented by Li et al. [44] and Su et al. [45], which depended on the neighbors' relative states. Unlike [46], this work considers an average consensus rather than a lead-following tracking synchronization based on an undirected graph for network topology.

Thanks to the above references for multiagent distributed control, this study has the following contributions:

(i) A basic synchronous controller is tested in multiple EHAs to realize the consensus of every EHA node with three-order nonlinear dynamics and an unknown external load. To the best of the authors' knowledge, this synchronous controller based on graph theory has not been applied to an electrohydraulic plant until now.

(ii) By using the feedback linearization method, the linear model of MEHAs is set up to conveniently design the synchronous consensus algorithm. Furthermore, a state-feedback matrix is derived from the pole placement technique, which is considered in the synchronous controller and improves the stable margin of MEHAs. Meanwhile, the general disturbance observer is adopted to estimate the external load.

(iii) Unlike many of the previous references, a two-DOF robotic bench driven by electrohydraulic actuators is used as the experimental bench for MEHAs with two nodes, which can verify the proposed synchronous consensus protocol.

This manuscript has the following organization. The multiple electrohydraulic motion model is constructed in Section 2. The synchronous control protocol is given in Section 3. The simulations and the experimental verification of MEHAs are given in Sections 4 and 5. Finally, the conclusion is drawn in Section 6.

2. Motion Plant Description

A synchronous control scheme for MEHAs' average consensus in a network topology based on undirected graph theory is described in Figure 1. Every electrohydraulic node has an isomorphic model and standalone control protocol. A MEHAs cooperation guarantees every EHA's consensus to their center balance state *O* using the synchronous control protocol design of the corresponding EHA.
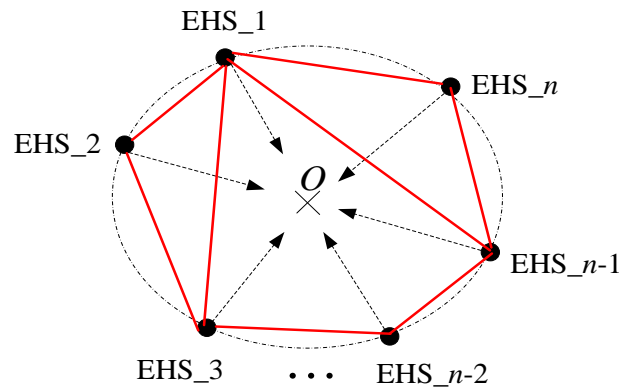
Figure 1. The synchronous control scheme for MEHAs' average consensus in a network topology based on undirected graph theory.

2.1. Nonlinear Dynamics of MEHAs

Jn Reference [47], the EHA had three system states such that $X_i = [x_{i1}, x_{i2}, x_{i3}]^T = [y, \dot{y}_i, A_p p_{Li}]^T$. Hence, the linear state space model for the ith EHA is described as

$$\begin{cases} \dot{x}_{i1} = x_{i2} \\ \dot{x}_{i2} = \dfrac{1}{m}(x_{i3} - Kx_{i1} - bx_{i2} - F_{Li}) \\ \dot{x}_{i3} = -\dfrac{4\beta_e A_p^2}{V_t}x_{i2} - \dfrac{4\beta_e C_{tl}}{V_t}x_{i3} \\ \qquad + \dfrac{4\beta_e C_d w K_{sv} A_p}{V_t \sqrt{\rho}}\sqrt{p_s - \mathrm{sgn}(u_i)x_{i3}/A_p}\,u_i \end{cases} , \quad i = 1, \dots, n \qquad (1)$$

where $\mathrm{sgn}(\cdot)$ is a signum function.

If the hydraulic parameters are assumed to be constant and a priori in every EHA model, then the model in (1) is rewritten as

$$\begin{cases} \dot{X}_i = AX_i + B\phi(x_{i3})u_i + D_{Li} \\ \qquad = f(X_i) + g(X_i)u_i + D_{Li} \\ y_i = CX_i = h(X_i) \end{cases} , \qquad (2)$$

where

$$A = \begin{bmatrix} 0 & 1 & 0 \\ -\theta_1 & -\theta_2 & \theta_3 \\ 0 & -\theta_4 & -\theta_5 \end{bmatrix}, B = \begin{bmatrix} 0 \\ 0 \\ \theta_6 \end{bmatrix}, D_{Li} = \begin{bmatrix} 0 \\ d_{Li} \\ 0 \end{bmatrix},$$

$C = [1, 0, 0], \theta_1 = K/m, \theta_2 = b/m, \theta_3 = 1/m, \theta_4 = 4\beta_e A_p^2/V_t, \theta_5 = 4\beta_e C_{tl}/V_t, \theta_6 = 4\beta_e C_d K_{sv} w A_p/(V_t\sqrt{\rho}), d_{Li} = -F_{Li}(t)/m, \phi(x_{i3}) = \sqrt{p_s - \mathrm{sgn}(u_i)x_{i3}/A_p}, f(X_i) = AX_i, g(X_i) = [0, 0, \theta_6\sqrt{p_s - \mathrm{sgn}(u_i)x_{i3}/A_p}]^T.$

Remark 1. *The function $\phi(x_{i3})$ is bounded and positive because the state x_{i3} yields $0 < p_r < x_3/A_p < p_s$.*

Assumption 1 ([11]). *The external load F_L is a variable disturbance that relies on the mechanical plant motion, i.e., $F_L(t) = F_L(t, X)$. However, F_L is bounded such that $|F_L(t)| \le F_{L\max}$, where $F_{L\max}$ is an unknown constant.*

2.2. Feedback Linearization Transformation

Consider the single-input and single-output systems for the ith EHA (2). Via the Lie derivative method [48], the precise feedback linearization model of MEHAs is derived using the following procedure.

At first, a new state vector is described such that $z_i = [z_{i1}, z_{i2}, z_{i3}]^T = [x_{i1}, x_{i2}, -\theta_1 x_{i1} - \theta_2 x_{i2} + \theta_3 x_{i3}]^T$. Because the derivative $\ddot{y}_i = -\theta_1 \dot{x}_{i1} - \theta_2 \dot{x}_{i2} + \theta_3 \dot{x}_{i3}$ includes the control u_i, the nonlinear model (2) has three relative orders. Therefore, $\dot{z}_{i1} = z_{i2}$, $\dot{z}_{i2} = z_{i3}$, and $\dot{z}_{i3}$ yield

$$
\begin{aligned}
\dot{z}_{i3} &= -\theta_1 \dot{x}_{i1} - \theta_2 \dot{x}_{i2} + \theta_3 \dot{x}_{i3} \\
&= \theta_1 \theta_2 x_{i1} - (\theta_1 - \theta_2^2 + \theta_3 \theta_4) x_{i2} - (\theta_2 \theta_3 + \theta_3 \theta_5) x_{i3} \\
&\quad + \theta_3 \theta_6 \sqrt{p_s - \text{sgn}(u_i) x_{i3} / A_p} \, u_i - \theta_2 d_{Li}
\end{aligned}
\tag{3}
$$

Secondly, the dynamic $\dot{z}_{i3}$ is linearized using the Lie derivative technique as follows:

$$
\begin{cases}
L_f h(X_i) = \dfrac{\partial h}{\partial x} f(X_i) = x_{i2} \\[2mm]
L_f^2 h(X_i) = \dfrac{\partial L_f h}{\partial X_i} f(X_i) = -\theta_1 x_{i1} - \theta_2 x_{i2} + \theta_3 x_{i3} \\[2mm]
L_f^3 h(X_i) = \dfrac{\partial L_f^2 h}{\partial X_i} f(X_i) = \theta_1 \theta_2 x_{i1} \\[2mm]
\qquad\qquad - (\theta_1 - \theta_2^2 + \theta_3 \theta_4) x_{i2} - (\theta_2 \theta_3 + \theta_3 \theta_5) x_{i3}
\end{cases}
\tag{4}
$$

In a linearized model, u_i in (2) is converted into the new control variable v_i, which has the following condition

$$
u_i = \alpha(X_i) + \gamma^{-1}(X_i) v_i
\tag{5}
$$

where

$$
\begin{aligned}
\alpha(X_i) &= -\dfrac{L_f^3 h}{L_g L_f^2 h} = -\dfrac{\theta_1 \theta_2 x_{i1} + (-\theta_1 + \theta_2^2 - \theta_3 \theta_4) x_{i2}}{\theta_3 \theta_6 \sqrt{p_s - \text{sgn}(u_i) x_{i3} / A_p}} \\
&\quad + \dfrac{(\theta_2 \theta_3 + \theta_3 \theta_5) x_{i3}}{\theta_3 \theta_6 \sqrt{p_s - \text{sgn}(u_i) x_{i3} / A_p}},
\end{aligned}
\tag{6}
$$

$$
\gamma(X_i) = L_g L_f^2 h = \theta_3 \theta_6 \sqrt{p_s - \text{sgn}(u_i) x_{i3} / A_p}.
$$

Hence, the feedback linearization model for (2) is derived as follows:

$$
\begin{cases}
\dot{z}_i = A_c z_i + B_c \gamma(X_i)[u_i - \alpha(X_i)] + \bar{D}_{Li} \\
y_i = C_c z_i
\end{cases}
\tag{7}
$$

where

$$
A_c = \begin{bmatrix} 0 & 1 & 0 \\ 0 & 0 & 1 \\ 0 & 0 & 0 \end{bmatrix}, \, B_c = \begin{bmatrix} 0 \\ 0 \\ 1 \end{bmatrix}, \, \bar{D}_{Li} = \begin{bmatrix} 0 \\ d_{Li} \\ -\theta_2 d_{Li} \end{bmatrix},
$$

$C_c = \begin{bmatrix} 1 & 0 & 0 \end{bmatrix}$.

In (5)–(7), the feedback linearization model of the MEHAs' nonlinear dynamics is described as

$$
\begin{cases}
\dot{z}_{i1} = z_{i2} \\
\dot{z}_{i2} = z_{i3} + d_{Li} \\
\dot{z}_{i3} = v_i - \theta_2 d_{Li} \\
y_i = z_{i1}
\end{cases}
\tag{8}
$$

and is standardized to the state space form

$$\dot{z}_i = A_c z_i + B_c v_i + \bar{D}_{Li}. \tag{9}$$

Remark 2. *The model in (9) is a precise linearization of the primary model in (1). Moreover, the control u_i in (5) and its transformed form v_i in (9) are inverse.*

3. Synchronous Protocol Derivation

For a compact denotation, the state vector of MEHAs $\xi = [\xi_1, \ldots, \xi_n]^T = [z_1, \ldots, z_n]^T \in \mathbb{R}^{3n \times 1}$ and the corresponding synchronous protocol $v = [v_1, \ldots, v_n]^T \in \mathbb{R}^n$ are defined. Then the state space model of MEHAs is given by

$$\dot{\xi} = (I_n \otimes A_c)\xi + (I_n \otimes B_c)v + \bar{D}_L, \tag{10}$$

where $\bar{D}_L = [\bar{D}_{L1}, \ldots, \bar{D}_{Ln}]^T \in \mathbb{R}^{3n \times 1}$.

Definition 1 ([49]). *A graph is a pair $(\mathcal{V}_n, \varepsilon_n)$, where $\mathcal{V}_n = 1, 2, \ldots, n$ is a finite nonempty node set and $\varepsilon_n \subseteq \mathcal{V}_n \times \subseteq \mathcal{V}_n$ is an edge set of ordered pairs of nodes. The edge (i, j) in the edge set of a directed graph denotes that vehicle j can obtain the information from vehicle i, i.e., $(i, j) \in \varepsilon_n$. If $(i, j) \in \varepsilon_n$, then the called weight of an edge $a_{ij} > 0$, else $a_{ij} = 0$. An undirected graph is a special case of a directed graph, where an edge (i, j) in the undirected graph corresponds to edges (i, j) and (j, i) in the directed graph. Then, a Laplacian matrix of MEHAs is defined as $\mathcal{L}_n = [l_{ij}] \in \mathbb{R}^{n \times n}$ as follows:*

$$l_{ii} = \sum_{j=1, j \neq i}^{n} a_{ij}, \qquad l_{ij} = -a_{ij}, \; i \neq j. \tag{11}$$

Since the external load $\bar{D}_L$ is unknown in (10), the disturbance observer $\hat{d}_L = [d_{L1}, \ldots, d_{Ln}]^T$ is designed as follows:

$$\dot{\hat{d}}_L = -Q_d^T (L_n^T \otimes B_c^T)e - M_d \hat{d}_L, \tag{12}$$

where M_d denotes a diagonal gain, Q_d is a state feedback gain of the disturbance observer, e is the transformation of the state vector ξ defined as $e = (\mathcal{L}_n \otimes P^{-1})\xi$, and P is a positive definite matrix to be selected.

The synchronous control protocol of the MEHAs is given by

$$\begin{aligned} v_i &= cK_v \sum_{j=1}^{n} a_{ij}(\xi_i - \xi_j) + \bar{K}_p \xi_i + q_i \hat{d}_{Li}, \; i = 1, \ldots n \\ &\Leftrightarrow v = (\mathcal{L}_n \otimes cK_v + I_n \otimes \bar{K}_p)\xi + Q_d \hat{d}_L \end{aligned}, \tag{13}$$

where $v = [v_1, \ldots, v_n]^T$, the constant $c = 1/\lambda_{\min}$, $\lambda_{\min}$ is the minimal eigenvalue of $\mathcal{L}_n$, $K_v = -B_c^T P^{-1}$, $\bar{K}_p$ is a state-feedback matrix using pole placement, and $Q_d = \text{diag}\{q_1, \ldots, q_n\}$.

Remark 3. *The MEHAs' consensus is directly guaranteed by the first item of v_i in (13). The second item $\bar{K}_p \xi_i$ is the pole configuration, which improves the system-stable margin of each EHA. The external disturbance $\bar{D}_{Li}$ is compensated for by the last item $q_i \hat{d}_{Li}$.*

Remark 4. *The state-feedback matrix $\bar{K}_p$ is used to transform the system matrix A_c into a stable system matrix $\bar{A}_c$ using pole placement as $\bar{A}_c = A_c + B_c \bar{K}_p$. In other words, the new system matrix's eigenvalues $\lambda(\bar{A}_c) < 0$.*

Theorem 1. *The MEHAs system in (10) involves the synchronous control protocol in (13) and the disturbance observer in (12) under Assumption 1. If there exists a positive definite matrix P, it yields*

$$\left(\bar{A}_c P + P \bar{A}_c^T + 2\delta I_3 - 2B_c B_c^T \right) + kP < 0, \tag{14}$$

where $\bar{A}_c = A_c + B_c\bar{K}_p$, δ and k are positive constants, then every node state $\|\xi_i(t) - \xi_j(t)\| < \sqrt{\Delta/(\alpha\lambda_{\min}(P^{-1}))}, (i, j = 1, \dots, n, i \neq j), t \to \infty$, where Δ is bounded and α is a positive constant, i.e., the protocol in (13) asymptotically achieves consensus to a zero neighborhood with an arbitrarily small size.

Proof. For the state vector ξ of the MEHAs in (10), the candidate Lyapunov function is chosen as follows:

$$
\begin{aligned}
V &= \frac{1}{2}\sum_{i=1}^{n}\left\{\left[\sum_{j=1}^{n}a_{ij}(\xi_i^T - \xi_j^T)P^{-1}\sum_{j=1}^{n}a_{ij}(\xi_i - \xi_j)\right] + \tilde{d}_{Li}^2\right\} \\
&= \frac{1}{2}[(\mathcal{L}_n \otimes I_3)\xi]^T\left[(I_n \otimes P^{-1})(\mathcal{L}_n \otimes I_3)\xi\right] + \frac{1}{2}\tilde{d}_L^T\tilde{d}_L \\
&= \frac{1}{2}e^T(I_n \otimes P)e + \frac{1}{2}\tilde{d}_L^T\tilde{d}_L
\end{aligned}
\tag{15}
$$

where the first evaluation item is the consensus errors of the MEHAs and the other item $\tilde{d}_L = d_L - \hat{d}_L$ is the observer estimation errors.

Then, the derivative $\dot{V}$ yields

$$
\begin{aligned}
\dot{V} &= \xi^T(\mathcal{L}_n^T \otimes I_3)(I_n \otimes P^{-1})(\mathcal{L} \otimes I_3)\dot{\xi} + \tilde{d}_L^T\dot{\tilde{d}}_L \\
&= \xi^T(\mathcal{L}_n^T \otimes I_3)(I_n \otimes P^{-1})(\mathcal{L}_n^T \otimes I_3)\cdot \\
&\quad [(I_n \otimes A_c)\xi + (I_n \otimes B_c)v + \bar{D}_L] + \tilde{d}_L^T\dot{\tilde{d}}_L
\end{aligned}
\tag{16}
$$

Substituting the synchronous control protocol in (13) into (17), $\dot{V}$ yields

$$
\begin{aligned}
\dot{V} &= \xi^T(\mathcal{L}_n^T \otimes I_3)(I_n \otimes P^{-1})(\mathcal{L}_n \otimes I_3)[(I_n \otimes A_c)\xi \\
&\quad + (I_n \otimes B_c)(I_n \otimes \bar{K}_p + \mathcal{L}_n \otimes cK_v)\xi \\
&\quad + (I_n \otimes B_c)Q_d\hat{d}_L + \bar{D}_L] + \tilde{d}_L^T\dot{\tilde{d}}_L \\
&= e^T(I_n \otimes ((A_c + B_c\bar{K}_p)P) + \mathcal{L}_n \otimes cB_vK_vP)e \\
&\quad + e^T(\mathcal{L}_n \otimes I_3)\bar{D}_L + e^T(\mathcal{L}_n \otimes B_c)Q_d\hat{d}_L + \tilde{d}_L^T(d_L - \hat{d}_L) \\
&\leq e^T(I_n \otimes (A_c + B_c\bar{K}_p)P + \mathcal{L}_n \otimes cB_vK_vP)e \\
&\quad + \frac{\delta}{2}e^Te + \frac{1}{2\delta}\bar{D}_L^T(\mathcal{L}_n^T\mathcal{L}_n \otimes I_3)\bar{D}_L + \frac{\delta}{2}e^Te \\
&\quad + \frac{1}{2\delta}d_L^TQ_d^T(\mathcal{L}_n^T\mathcal{L}_n \otimes B_c^TB_c)Q_dd_L \\
&\quad - e^T(\mathcal{L}_n \otimes B_c)Q_d\tilde{d}_L - \tilde{d}_L^T\dot{\hat{d}}_L + \tilde{d}_L^T\dot{d}_L \\
&\leq \frac{1}{2}e^T(I_n \otimes ((A_c + B_c\bar{K}_p)P + P(A_c + B_c\bar{K}_p)^T \\
&\quad + 2\delta I_3) + 2\mathcal{L}_n \otimes cB_cK_vP)e + \frac{1}{2\delta}\bar{D}_L^T(\mathcal{L}_n^T\mathcal{L}_n \otimes I_3)\bar{D}_L \\
&\quad + \frac{1}{2\delta}d_L^TQ_d^T(\mathcal{L}_n^T\mathcal{L}_n \otimes B_c^TB_c)Q_dd_L \\
&\quad - \tilde{d}_L^T[\dot{\hat{d}}_L + Q_d^T(\mathcal{L}_n^T \otimes B_c^T)e] + \frac{1}{2}\tilde{d}_L^T\tilde{d}_L + \frac{1}{2}d_L^Td_L \\
&= \frac{1}{2}e^T\left(I_n \otimes \left(\bar{A}_cP + P\bar{A}_c^T + 2\delta I_3\right) + 2\mathcal{L}_n \otimes cB_cK_vP\right)e \\
&\quad - \tilde{d}_L^T[\dot{\hat{d}}_L + Q^T(\mathcal{L}_n^T \otimes B^T)e]\frac{1}{2\delta}d_L^T[(1 + \theta_2^2)\mathcal{L}_n^T\mathcal{L}_n \\
&\quad + Q_d^T(\mathcal{L}_n^T\mathcal{L}_n \otimes B_c^TB_c)Q_d]d_L + \frac{1}{2}\tilde{d}_L^T\tilde{d}_L + \frac{1}{2}d_L^Td_L
\end{aligned}
\tag{17}
$$

where

$$
\begin{aligned}
\bar{D}_L^T &(\mathcal{L}_n^T \mathcal{L}_n \otimes I_3) \bar{D}_L \\
&= (d_L^T \mathcal{L}_n^T \mathcal{L}_n \otimes \begin{bmatrix} 0 & 1 & -\theta_2 \end{bmatrix})(d_L \otimes \begin{bmatrix} 0 & 1 & -\theta_2 \end{bmatrix}^T) \\
&= d_L^T \mathcal{L}_n^T \mathcal{L}_n d_L \otimes (1 + \theta_2^2) \\
&= (1 + \theta_2^2) d_L^T \mathcal{L}_n^T \mathcal{L}_n d_L
\end{aligned}
\tag{18}
$$

Let $\Delta = \frac{1}{2\delta} d_L^T[(1 + \theta_2^2)\mathcal{L}_n^T \mathcal{L}_n + Q_d^T(\mathcal{L}_n^T \mathcal{L}_n \otimes B_c^T B_c)Q_d + \delta M_d^T M_d] d_L + \frac{1}{2} d_L^T d_L$, and substituting the disturbance observer in (12) into (17), $\dot{V}$ is given by

$$
\begin{aligned}
\dot{V} =\ & \frac{1}{2} e^T (I_n \otimes (\bar{A}_c P + P\bar{A}_c^T + 2\delta I_3) + 2\mathcal{L}_n \otimes cB_c K_v P) e \\
& + \tilde{d}_L^T M_d \hat{d}_L + \frac{1}{2\delta} d_L^T[(1 + \theta_2^2)L_n^T \mathcal{L}_n \\
& + Q_d^T(\mathcal{L}_n^T \mathcal{L}_n \otimes B_c^T B_c)Q_d] d_L + \frac{1}{2} \tilde{d}_L^T \tilde{d}_L + \frac{1}{2} d_L^T d_L \\
\leq\ & \frac{1}{2} e^T (I_n \otimes (\bar{A}_c P + P\bar{A}_c^T + 2\delta I_3) + 2\mathcal{L}_n \otimes cB_c K_v P) e \\
& - \tilde{d}_L^T (M_d - I_n) \tilde{d}_L + \Delta
\end{aligned}
\tag{19}
$$

In (19), the item $2\mathcal{L}_n \otimes cB_c K_v P$ involves the unknown variable matrix P and the specified matrix K_v. If K_v is designed as $K_v = -B_c^T P^{-1}$, then the first item in (19) is converted into an LMI as follows:

$$
\begin{aligned}
\dot{V} \leq\ & \frac{1}{2} e^T (I_n \otimes (\bar{A}_c P + P\bar{A}_c^T + 2\delta I_3) - 2\mathcal{L}_n \otimes cB_c B_c^T) e \\
& - \tilde{d}_L^T (M_d - I_n) \tilde{d}_L + \Delta
\end{aligned}
\tag{20}
$$

For the Laplacian matrix $\mathcal{L}_n$ of MEHAs, there exists an orthogonal matrix U such that $U^T \mathcal{L}_n U = \Lambda$, where Λ is a diagonal matrix. Then, a linear transformation is defined as $\tilde{e} = (U \otimes I_m)e$, and $\dot{V}$ is rewritten as

$$
\begin{aligned}
\dot{V} \leq\ & \frac{1}{2} e^T ((U^T \otimes I_m)[I_n \otimes (\bar{A}_c P + P\bar{A}_c^T + 2\delta I_3)](U \otimes I_m) \\
& - 2(U^T \otimes I_m)(UL_n U^T \otimes cB_c B_c^T)(U \otimes I_m)) e \\
& - \tilde{d}_L^T (M_d - I_n) \tilde{d}_L + \Delta \\
\leq\ & \frac{1}{2} \tilde{e}^T (I_n \otimes (\bar{A}_c P + P\bar{A}_c^T + 2\delta I_3) \\
& - 2I_n \lambda_{\min} \otimes cB_c B_c^T) \tilde{e} - \tilde{d}_L^T (M_d - I_n) \tilde{d}_L + \Delta \\
=\ & \frac{1}{2} e^T (I_n \otimes (\bar{A}_c P + P\bar{A}_c^T + 2\delta I_3 - 2c\lambda_{\min} B_c B_c^T)) e \\
& - \tilde{d}_L^T (M_d - I_n) \tilde{d}_L + \Delta
\end{aligned}
\tag{21}
$$

where $\lambda_{\min}$ is the minimal eigenvalue of $\mathcal{L}_n$, except for the only zero eigenvalue.

Since the constant c is designed as $c = 1/\lambda_{\min}$ in (13), according to the LMI condition (14), $\dot{V}$ yields

$$
\dot{V} \leq -\frac{k}{2} e^T (I_n \otimes P) e - \frac{1}{2} \tilde{d}_L^T[2(M_d - I_n)] \tilde{d}_L + \Delta.
\tag{22}
$$

Let $\alpha = \min\{k\lambda_{\min}(I_n \otimes P), 2\lambda_{\min}(M_d - I_n)\}$; $\dot{V}$ satisfies

$$
\dot{V} \leq -\alpha V + \Delta.
\tag{23}
$$

Integrate the two sides of (23) and V yields

$$
\begin{aligned}
V(t) &\leq V(0)e^{-\alpha t} + \int_0^t \Delta e^{-\alpha(t-\varepsilon)} d\varepsilon \\
&\leq V(0)e^{-\alpha t} + \Delta(1 - e^{-\alpha t})/\alpha
\end{aligned}
\tag{24}
$$

Now, from (24), let $t \to \infty$, the convergence domain for the MEHAs' synchronous error is $H_r = \sqrt{\Delta/(\alpha\lambda_{\min}(P^{-1}))}$. Furthermore, the dimension of H_r mainly relies on the magnitude Δ/α. Thus, the larger constant k and the smaller constant α can reduce the dimension of H_r when $t \to \infty$. □

Figure 2 shows the flow chart of the average consensus control scheme of the MEHAs. The MEHAs' nonlinear dynamics are set up (2). Using the feedback linearization method, the MEHAs' linear form is represented (9), from which the state space model of the MEHAs is derived (10). To address the unknown external load, the disturbance observer (12) is designed and compensated for in the synchronous control protocol (13). This synchronous protocol is based on the undirected graph shown in Figure 1, which means that each node can share its respective information. The objective of the proposed synchronous protocol is to guarantee the state consensus of all nodes.
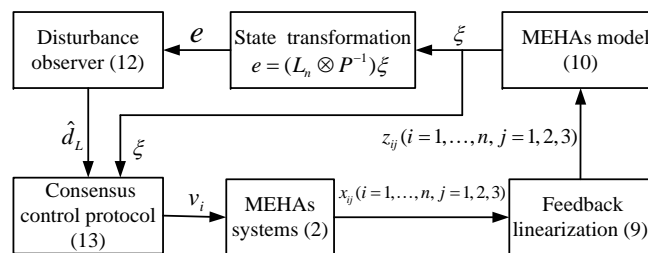

Figure 2. The flow chart of the average consensus control scheme

4. Simulation Results

For the convenience and consistency of the following experiments, two EHAs are simulated to verify the proposed synchronous control scheme. Some model parameters of MEHAs are given by $\theta_1 = 500$, $\theta_2 = 50$, $\theta_3 = 0.5$, $\theta_4 = 5.63 \times 10^5$, $\theta_5 = 348$, $\theta_6 = 1.13 \times 10^3$, $p_s = 40$ bar, $p_r = 2$ bar, and $A_p = 4.91$ cm^2. The two external load disturbances are assumed to be $F_{L1} = 0.5\sin(0.5\pi t)$ and $F_{L2} = 0.3\sin(0.5\pi t)$. The disturbance observer parameters are $Q_d = \text{diag}\{10, 10\}$ and $M_d = \text{diag}\{4, 4\}$. The synchronous control parameters are $\mathcal{L}_n = [1, -1; 1, -1]$, $c = 1/2$, $k = 1$, $\delta = 0.1$, and $P = [0.14, -0.33, -0.14; -0.33, 1.03, -1.47; -0.14, -1.47, 15.89]$. The state-feedback matrix is $\bar{K}_p = \bar{K}_{p1} = [-600, -250, -29]$ and its corresponding pole placement is $\lambda_1(\bar{A}_c) = [-10, -15, -4]$ for the matrix A_c. The initial values of the two EHAs are $x_{11}(0) = 30$ mm, $x_{12}(0) = 10$ mm/s, $x_{13}(0) = 100$ N, $x_{21}(0) = -20$ mm, $x_{22}(0) = -10$ mm/s, and $x_{23}(0) = -100$ N.

4.1. Simulation Verification of the Two Nodes

The simulation results of the average consensus controller are shown in Figures 3–5. Since MEHAs have an undirected topology, as shown in Figure 1, the corresponding state responses of the two nodes achieved consensus, as shown in Figure 3. In other words, the synchronous state errors involving the cylinder position error $x_{11} - x_{21}$, the velocity error $x_{12} - x_{22}$, and the load pressure error $x_{13} - x_{23}$ converged to zero using the synchronous control protocol (13), as shown in Figure 4. In addition, by using the disturbance observer (12), the disturbance estimation $\hat{d}_{Li}$ is well regulated to track the real disturbance value d_{Li} with a satisfactory disturbance estimation error $\tilde{d}_{Li}$, as shown in Figure 5.
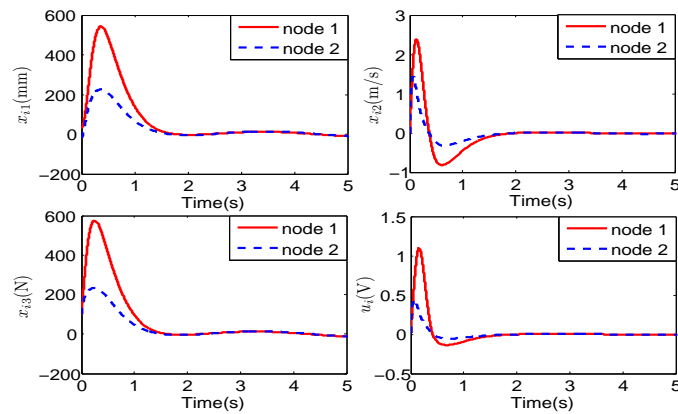
Figure 3. The MEHAs' state responses of the two nodes in the simulation: x_{i1}—the cylinder position; x_{i2}—the cylinder velocity; x_{i3}—the cylinder load pressure; u_i—the control voltage of the servo valve.
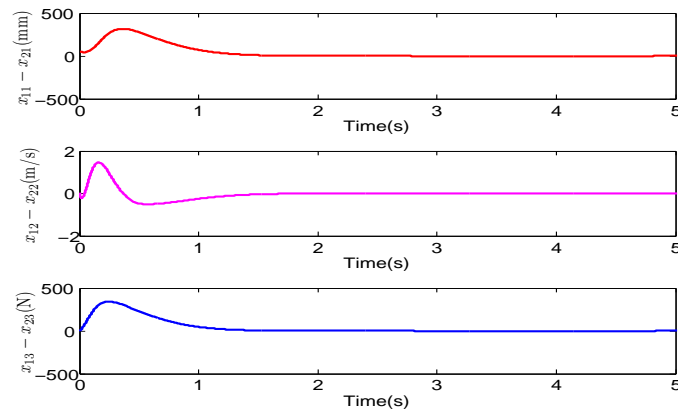

Figure 4. The MEHAs' state errors of the two nodes in the simulation: $x_{11} - x_{21}$ (the red line) —the cylinder position error; $x_{12} - x_{22}$ (the pink line) —the cylinder velocity error; $x_{13} - x_{23}$ (the blue line) —the cylinder load pressure error.
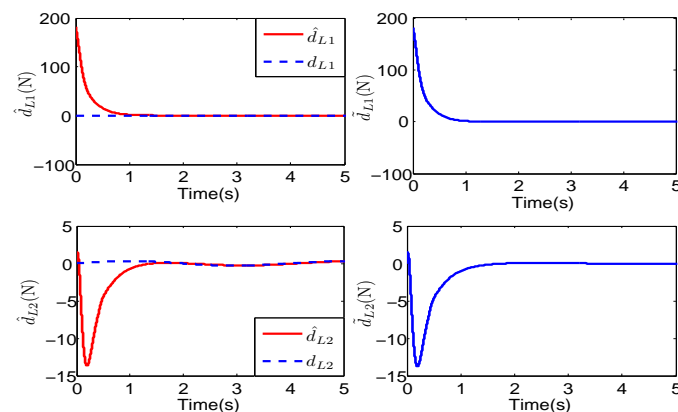

Figure 5. The disturbance observers and their corresponding errors of the two nodes in the simulation: d_{Li} is the disturbance actual value, $\hat{d}_{Li}$ is the disturbance observer estimation, $\tilde{d}_{Li}$ is the disturbance estimation error.

4.2. Comparison with Different State-Feedback Matrices

To analyze the consensus rate of the two nodes, the other two state-feedback matrices mentioned in the synchronous control protocol (13) are selected as $\bar{K}_{p2} = [-2400, -580, -43]$ and $\bar{K}_{p3} = [-5250, -1025, -60]$. The respective pole placements are $\lambda_2(\bar{A}_c) = \{-15, -20, -8\}$ and $\lambda_3(\bar{A}_c) = \{-35, -15, -10\}$. The corresponding comparative state response results are shown in Figures 6–8. The consensus rate with the state-feedback matrix $\bar{K}_p = \bar{K}_{p3}$ was

faster than that of the other two conditions since its matrix had the largest gain elements among the three conditions. In other words, the larger the state-feedback gain $\bar{K}_p$, the faster the consensus rate. Furthermore, the three steady-state errors $|x_{1i} - x_{2i}|(i = 1, 2, 3)$ with respect to the largest matrix gain $\bar{K}_{p3}$ were less than those of the other two conditions, which indicates the favorable consensus effect using the proposed synchronous control protocol.
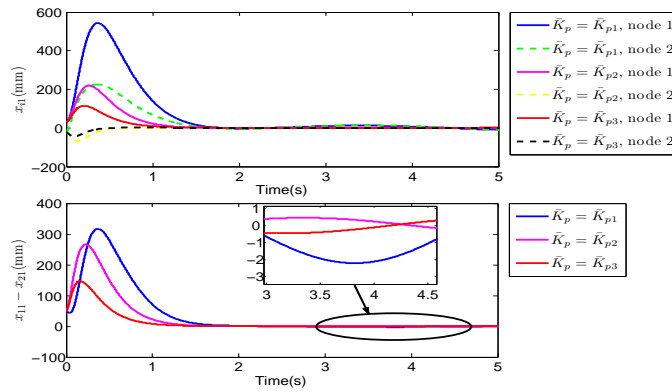

Figure 6. The comparative position response results of the three state-feedback matrixes using pole placement in the simulation.
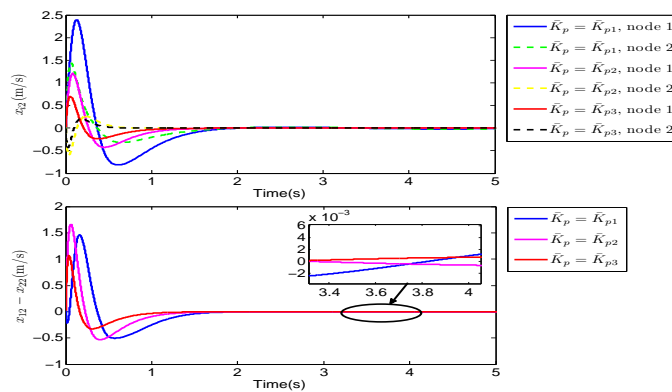

Figure 7. The comparative velocity response results of the three state-feedback matrices using pole placement in the simulation.
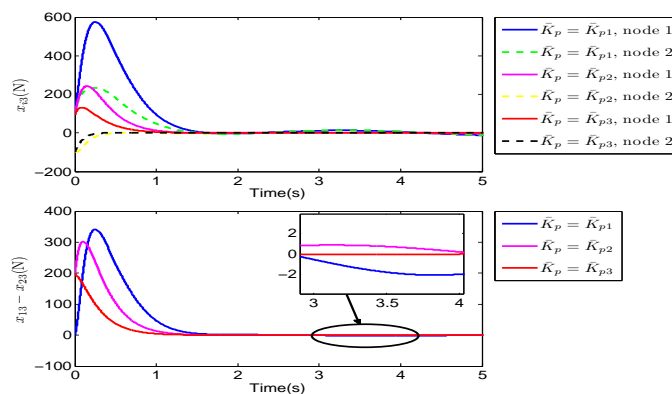

Figure 8. The comparative pressure response results of the three state-feedback matrices using pole placement in the simulation.

5. Experimental Verification

To verify the synchronous control scheme for MEHAs, the experimental bench with two electrohydraulic actuator nodes is built, which is shown in Figure 9. Each EHA node is composed of a servo valve and a hydraulic cylinder, respectively, which drive the robotic upper arm and forearm motion simultaneously. In fact, the dynamics of the two robotic arms become the two external loads of the MEHAs. The MEHAs' three states are measured by the displacement and pressure transducers, respectively. The measured resolutions for the displacement and pressure transducers are less than 10^{-3}. The range of the hydraulic cylinder is 80 mm due to the joint constraints of the robotic arm. An accumulator is adopted to supply the hydraulic transient flow. The disturbance observer parameters are $Q_d = \mathrm{diag}\{30, 30\}$ and $M_d = \mathrm{diag}\{2, 2\}$. The synchronous control parameters are $\mathcal{L}_n = [1, -1; 1, -1]$, $\bar{K}_p = \bar{K}_{pb} = [-4400, -860, -52]$, $c = 1/2$, $k = 1$, $\delta = 0.01$, and $P = [0.39, -2.02, 0.18; -2.02, 12.76, -30.9; 0.18, -30.9, 502.6]$. The initial values of the two EHAs are $x_{11}(0) = -11$ mm, $x_{12}(0) = 0$ mm/s, $x_{13}(0) = -324$ N, $x_{21}(0) = 67$ mm, and $x_{22}(0) = 0$ mm/s, $x_{23}(0) = -325$ N.

5.1. Experimental Verification of Two Nodes

The MEHAs' state responses of the two nodes in the experiment are shown in Figure 10. The nodes 1 and 2 EHAs drive the robotic upper arm and the forearm rotations, respectively. After 2 s, a consensus is achieved using the proposed synchronous control protocol. The steady-state pressures x_{13} and x_{23} of the two nodes are not close to zero since the existing external loads should be compensated for by x_{i3} from the driving force of the two robotic arms. Note that 8.5 s later, two cylinder positions gradually approach the zero point (mechanical balance state) due to the gravities of the two robotic arms. Meanwhile, the load pressure of the robotic upper arm is increased to hold the two static gravities of both robotic arms. Hence, the load pressure errors of the two nodes $|x_{13} - x_{23}|$ are of greater magnitudes than the corresponding position and velocity errors $|x_{1i} - x_{2i}|(i = 1, 2)$, as shown in Figure 11. At the mechanical balance states, the control voltages of the servo valve are zero, which means that the two hydraulic flows are cut off to supply the constant load pressures for the respective gravities of the robotic arms.

5.2. Experimental Comparison Results

Similar to the simulation comparison, the other two state-feedback matrices are selected as $\bar{K}_{pa} = [-1200, -395, -36]$ and $\bar{K}_{pc} = [-6000, -1150, -65]$. Certainly, the corresponding initial state values could also be selected as (1) $x_{11}(0) = 42$ mm, $x_{12}(0) = 0$ mm/s, $x_{13}(0) = 340$ N, $x_{21}(0) = -8$ mm, $x_{22}(0) = 0$ mm/s, and $x_{23}(0) = 383$ N; (2) $x_{11}(0) = -11$ mm, $x_{12}(0) = 0$ mm/s, $x_{13}(0) = -345$ N, $x_{21}(0) = 69$ mm, $x_{22}(0) = 0$ mm/s, and $x_{23}(0) = -323$ N. The corresponding comparative state responses are shown in Figures 12–14. Since the state-feedback matrix $\bar{K}_{pc}$ had the largest gain elements, its consensus rate was faster than the other two conditions, which is consistent with the simulation. Meanwhile, the steady-state error $|x_{11} - x_{21}| < 2$ mm with respect to the largest matrix gain $\bar{K}_{pc}$ verified the effectiveness of the proposed synchronous control protocol. The steady velocity values of the two nodes entirely approached zero for the three conditions, as shown in Figure 13. Note that in the fast-response condition (i.e., $\bar{K}_p = \bar{K}_{pc}$), the load pressure error of the two nodes $x_{13} - x_{23}$ was quickly reduced from 2600 N to 400 N, as shown in Figure 14, since the supply pressure of the hydraulic pumps was relieved by the relief valve. This operation can reduce the scattering loss of the EHSS.
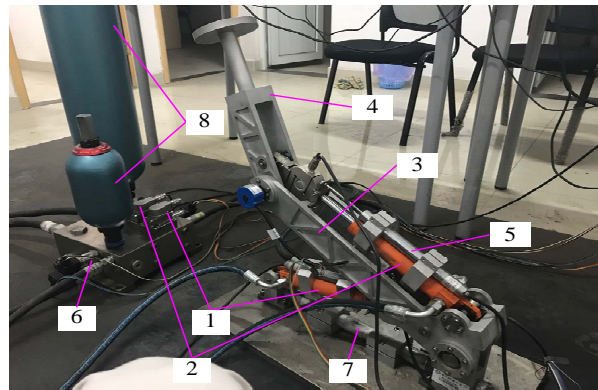
Figure 9. The experimental bench construction of the MEHAs with two EHA nodes: 1—node 1 (servo valve 1 and hydraulic cylinder 1); 2—node 2 (servo valve 2 and hydraulic cylinder 2); 3—robotic upper arm; 4—robotic forearm; 5—displacement transducer; 6—pressure transducer; 7—bench torso; 8—accumulator.
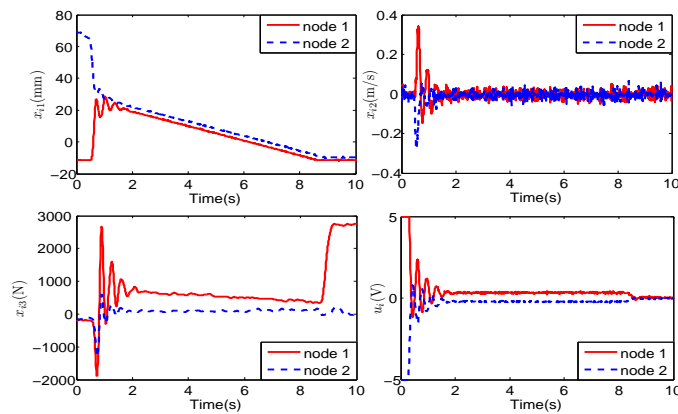

Figure 10. The MEHAs' state responses with two nodes in the experiment: x_{i1}—the cylinder position; x_{i2}—the cylinder velocity; x_{i3}—the cylinder load pressure; u_i—the control voltage of the servo valve.
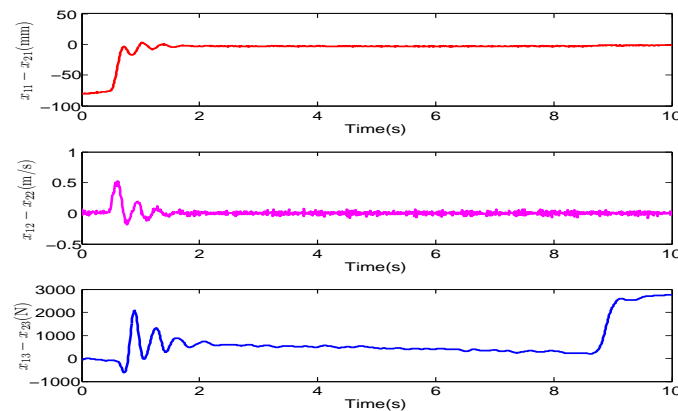

Figure 11. The MEHAs' state errors of two nodes in the experiment: $x_{11} - x_{21}$ (the red line)—the cylinder position error; $x_{12} - x_{22}$ (the pink line)—the cylinder velocity error; $x_{13} - x_{23}$ (the blue line)—the cylinder load pressure error.
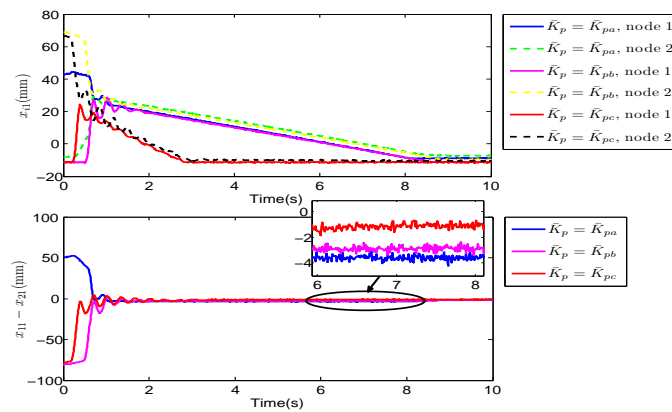
Figure 12. The compared position response results of the three state-feedback matrices using pole placement in the experiment.
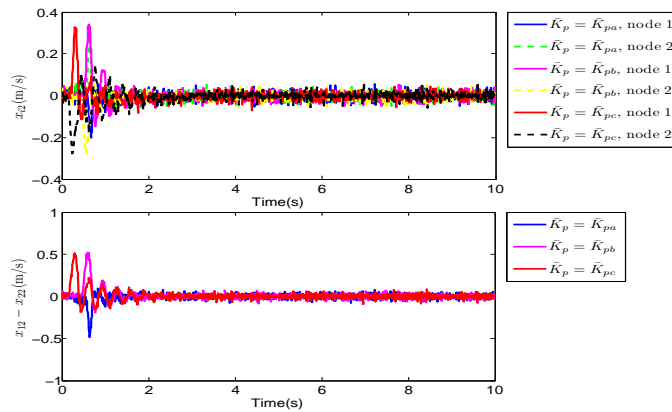

Figure 13. The compared velocity response results of the three state-feedback matrices using pole placement in the experiment.
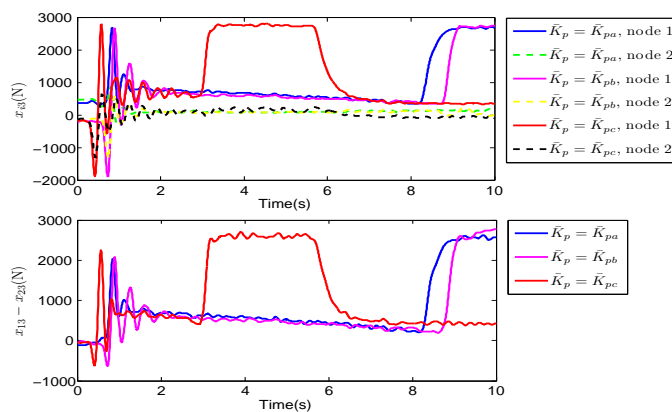

Figure 14. The compared pressure response results of the three state-feedback matrices using pole placement in the experiment.

6. Conclusions

In this study, a synchronous controller is used in multiple electrohydraulic actuators to realize the average consensus of every EHA node based on undirected graph theory. The feedback linearization model of the EHA with external load disturbance is set up to derive the linear state space model of MEHAs. Then, the synchronous control protocol is designed based on undirected network topology. Finally, a two-DOF robotic bench is set up to verify the effectiveness of the distributed control scheme. To be honest, the EHA nodes in this study are not adequate due to the robotic bench constraints. However, the

proposed synchronous control method can be promoted in general mechatronic systems driven by multiple electrohydraulic actuators based on graph theory and cooperative control protocol. In the future, distributed synchronous control will be investigated based on directed spanning-tree topology and communication delays.

Author Contributions: J.Q. was in charge of the writing of this article; Q.G. and Y.Y. conceived and designed the architecture of this paper; H.R. corrected the text; Z.C. and D.J. performed the simulations and experiments. All authors have read and agreed to the published version of the manuscript.

Conflicts of Interest: The authors declare no conflict of interest.

Nomenclature

C_d	Discharge coefficient of the servo valve
w	Area gradient of the servo valve
p_s, p_r	Supply pressure and return pressure
p_L	Load pressure of the hydraulic cylinder
ρ	Density of the hydraulic oil
C_{tl}	Total leakage coefficient of the hydraulic cylinder
β_e	Effective bulk modulus
A_p	Annulus area of the hydraulic cylinder chamber
V_t	Total volume of the hydraulic power mechanism
K	Spring stiffness coefficient of the hydraulic cylinder
m, b	Load mass and viscous damping coefficients
F_L	External load of the electrohydraulic system
K_{sv}, u	Gain and control voltage of the servo valve
$\otimes$	Kronecker product for the matrix
I_n	Identity matrix with n orders

References

1. Yang, Y.; Ma, L.; Huang, D. Development and repetitive learning control of lower limb exoskeleton driven by electro-hydraulic actuators. *IEEE Trans. Ind. Electron.* **2017**, *64*, 4169–4178. [CrossRef]
2. Chen, G.; Wang, J.; Wang, S.; Zhao, J.; Shen, W. Compliance control for a hydraulic bouncing system. *ISA Trans.* **2018**, *79*, 232–238. [CrossRef] [PubMed]
3. Semini, C.; Barasuol, V.; Goldsmith, J.; Frigerio, M.; Focchi, M.; Gao, Y.; Caldwell, D.G. Design of the hydraulically actuated, torque-controlled quadruped robot HyQ2Max. *IEEE/ASME Trans. Mechatronics* **2017**, *22*, 635–646. [CrossRef]
4. Koivumäki, J.; Mattila, J. Stability-guaranteed impedance control of hydraulic robotic manipulators. *IEEE/ASME Trans. Mechatronics* **2017**, *22*, 601–612. [CrossRef]
5. Shen, G.; Zhu, Z.; Zhao, J.; Zhu, W.; Tang, Y.; Li, X. Real-time tracking control of electro-hydraulic force servo systems using offline feedback control and adaptive control. *ISA Trans.* **2017**, *67*, 356–370. [CrossRef]
6. Guo, Q.; Chen, Z.; Shi, Y.; Yan, Y.; Guo, F. Synchronous control of multiple electrohydraulic actuators under distributed switching topologies with lumped uncertainty. *J. Franklin Inst.* **2022**, *359*, 4288–4306. [CrossRef]
7. Yao, J.; Deng, W.; Sun, W. Precision motion control for electro-hydraulic servo systems with noise alleviation: A desired compensation adaptive approach. *IEEE/ASME Trans. Mechatronics* **2017**, *22*, 1859–1868. [CrossRef]
8. Tran, D.T.; Ba, D.X.; Ahn, K.K. Adaptive backstepping sliding mode control for equilibrium position tracking of an electrohydraulic elastic manipulator. *IEEE Trans. Ind. Electron.* **2020**, *67*, 3860–3869. [CrossRef]
9. Guo, Q.; Zuo, Z.; Ding, Z. Parametric adaptive control of single-rod electrohydraulic system with block-strict-feedback model. *Automatica* **2020**, *113*, 108807. [CrossRef]
10. Yang, C.; Jiang, Y.; Li, Z.; He, W.; Su, C.Y. Neural control of bimanual robots with guaranteed global stability and motion precision. *IEEE Trans. Ind. Informat.* **2017**, *13*, 1162–1171. [CrossRef]
11. Kim, W.; Shin, D.; Won, D.; Chung, C.C. Disturbance-observer-based position tracking controller in the presence of biased sinusoidal disturbance for Electrohydraulic actuators. *IEEE Trans. Control Syst. Technol.* **2013**, *21*, 2290–2298. [CrossRef]
12. Guo, Q.; Chen, Z. Neural adaptive control of single-rod electrohydraulic system with lumped uncertainty. *Mech. Syst. Signal Proc.* **2021**, *146*, 106869. [CrossRef]
13. Li, S.; Wei, J.; Guo, K.; Zhu, W. Nonlinear robust prediction control of hybrid active-passive heave compensator with extended disturbance observer. *IEEE Trans. Ind. Electron.* **2017**, *64*, 6684–6694. [CrossRef]

14. He, W.; Meng, T.; Huang, D.; Li, X. Adaptive boundary iterative learning control for an Euler-Bernoulli beam system with input constraint. *IEEE Trans. Neural Netw. Learn. Syst.* **2018**, *29*, 1539–1549. [CrossRef] [PubMed]

15. Guo, Q.; Zhang, Y.; Celler, B.G.; Su, S.W. Neural adaptive backstepping control of a robotic manipulator with prescribed performance constraint. *IEEE Trans. Neural Netw. Learn. Syst.* **2019**, *30*, 3572–3583. [CrossRef] [PubMed]

16. Zheng, D.; Xu, H. Adaptive backstepping-flatness control based on an adaptive state observer for a torque tracking electrohydraulic system. *IEEE/ASME Trans. Mechatronics* **2016**, *21*, 2440–2452. [CrossRef]

17. Wang, N.; Xu, L.; Xie, F.; Shi, Y.; Wang, Y. Research on the dynamic characteristics of pneumatic proportional regulator in pneumatic-loading system and design of fuzzy adaptive controller. *Sci. China Technol. Sci.* **2022**, *65*, 956–965. [CrossRef]

18. Ning, F.; Shi, Y.; Cai, Y.; Xu, W. Research and application progress of data mining technology in electric power system. *J. Adv. Mfg. Sci. Technol.* **2021**, *1*, 2021007. [CrossRef]

19. Yao, J.; Di, D.; Jiang, G.; Gao, S.; Yan, H. Real-time acceleration harmonics estimation for an electro-hydraulic servo shaking table using Kalman Filter with a linear model. *IEEE Trans. Control Syst. Technol.* **2014**, *22*, 794–800. [CrossRef]

20. Yang, C.; Qu, Z.; Han, J. Decoupled-space control and experimental evaluation of spatial electrohydraulic robotic manipulators using singular value decomposition algorithms. *IEEE Trans. Ind. Electron.* **2014**, *61*, 3427–3438. [CrossRef]

21. Jafari, M.; Xu, H. A biologically-inspired intelligent controller for distributed velocity control of multiple electro-Hydraulic servo-systems. In Proceedings of the Symposium Series on Computational Intelligence, Honolulu, HI, USA, 27 November–1 December 2017 .

22. Cao, Y.; Yu, W.; Ren, W.; Chen, G. An overview of recent progress in the study of distributed multi-agent coordination. *IEEE Trans. Autom. Control* **2013**, *9*, 427–438. [CrossRef]

23. Lawton, J.R.; Beard, R.W. Synchronized multiple spacecraft rotations. *Automatica* **2002**, *38*, 1359–1364. [CrossRef]

24. Olfati-Saber, R.; Shamma, J.S. Consensus filters for sensor networks and distributed sensor fusion. In Proceedings of the IEEE Conference Decision Control & European Control Conference, Seville, Spain, 12–15 December 2015; pp. 6698–6703.

25. Ren, W.; Beard, R.W. Information consensus in multivehicle cooperative control. *IEEE Control Syst. Mag.* **2007**, *27*, 71–82.

26. Fax, J.A.; Murray, R.M. Information flow and cooperative control of vehicle formations. *IEEE Trans. Autom. Control* **2004**, *49*, 115–120. [CrossRef]

27. Su, H.; Wang, X.; Lin, Z. Flocking of multi-agents with a virtual leader. *IEEE Trans. Autom. Control* **2009**, *54*, 293–307. [CrossRef]

28. Olfati-Saber, R.; Fax, J.A.; Murray, R.M. Consensus and cooperation in networked multi-agent systems. *Proc. IEEE* **2007**, *95*, 215–233. [CrossRef]

29. Hong, Y.; Hu, J.; Gao, L. Tracking control for multi-agent consensus with an active leader and variable topology. *Automatica* **2006**, *42*, 1177–1182. [CrossRef]

30. Li, Z.; Liu, X.; Ren, W.; Xie, L. Consensus control of linear multi-agent systems with distributed adaptive protocols. In Proceedings of the American Control Conference, Montreal, QC, Canada, 27–29 June 2012; pp. 1573–1578.

31. Li, Z.; Ren, W.; Liu, X. Consensus of multi-agent systems with general linear and lipschitz nonlinear dynamics using distributed adaptive protocols. *IEEE Trans. Autom. Control* **2013**, *58*, 1786–1791. [CrossRef]

32. Zhang, H.; Lewis, F.L. Adaptive cooperative tracking control of higher-order nonlinear systems with unknown dynamics. *Automatica* **2012**, *48*, 1432–1439. [CrossRef]

33. Wen, G.; Duan, Z.; Yu, W.; Chen, G. Consensus of multi-agent systems with nonlinear dynamics and sampled-data information: A delayed-input approach. *Int. J. Robust Nonlin.* **2013**, *23*, 602–619. [CrossRef]

34. Zuo, Z.; Lin, T. A new class of finite-time nonlinear consensus protocols for multi-agent systems. *Int. J. Control Autom.* **2014**, *87*, 363–370. [CrossRef]

35. Ma, C.; Zhang, J. Necessary and sufficient conditions for consensusability of linear multi-agent systems. *IEEE Trans. Autom. Control* **2010**, *55*, 1263–1268.

36. Yu, W.; Lewis, F.L. Some necessary and sufficient conditions for second-order consensus in multi-agent dynamical systems. *Automatica* **2010**, *46*, 1089–1095. [CrossRef]

37. Lin, P.; Jia, Y. Average consensus in networks of multi-agents with both switching topology and coupling time-delay. *Physica A* **2008**, *387*, 303–313. [CrossRef]

38. Xiao, F.; Wang, L. Asynchronous consensus in continuous-time multi-agent systems with switching topology and time-varying delays. *IEEE Trans. Autom. Control* **2008**, *53*, 1804–1816. [CrossRef]

39. Wei, N.; Cheng, D. Leader-following consensus of multi-agent systems under fixed and switching topologies. *Syst. Control. Lett.* **2010**, *59*, 209–217.

40. Wen, G.; Duan, Z.; Ren, W.; Chen, G. Distributed consensus of multi-agent systems with general linear node dynamics and intermittent communications. *Int. J. Robust Nonlin.* **2014**, *24*, 2438–2457. [CrossRef]

41. Seo, J.; Shim, H.; Back, J. Consensus of high-order linear systems using dynamic output feedback compensator: Low gain approach. *Automatica* **2009**, *45*, 2659–2664. [CrossRef]

42. Li, Z.; Duan, Z.; Chen, G.; Huang, L. Consensus of multiagent systems and synchronization of complex networks: A unified viewpoint. *IEEE Trans. Circuits I* **2010**, *57*, 213–224.

43. Li, Z.; Liu, X.; Lin, P.; Ren, W. Consensus of linear multi-agent systems with reduced-order observer-based protocols. *Syst. Control. Lett.* **2011**, *60*, 510–516. [CrossRef]

44. Li, Z.; Wen, G.; Duan, Z.; Ren, W. Designing fully distributed consensus protocols for linear multi-agent systems with directed graphs. *IEEE Trans. Autom. Control* **2015**, *60*, 1152–1157. [CrossRef]
45. Su, H.; Chen, G.; Wang, X.; Lin, Z. Adaptive second-order consensus of networked mobile agents with nonlinear dynamics. *Automatica* **2011**, *47*, 368–375. [CrossRef]
46. Guo, Q.; Chen, Z.; Shi, Y.; Li, X.; Yan, Y.; Guo, F.; Li, S. Synchronous control for multiple electrohydraulic actuators with feedback linearization. *Mech. Syst. Signal Proc.* **2022**, *178*, 109280. [CrossRef]
47. Merritt, H. *Hydraulic Control Systems*; John Wiley & Sons: New York, NY, USA, 1967.
48. Khalil, H.K. *Nonlinear Systems*, 3rd ed.; Prentice Hall: Upper Saddle River, NJ, USA, 2002.
49. Ren, W.; Beard, R.W. *Distributed Consensus in Multi-Vehicle Cooperative Control Theory and Applications*; Springer: London, UK, 2008.